ACS APPLIED MATERIALS & INTERFACES

Research Article

www.acsami.org

γ-Alumina Modification with Long Chain Carboxylic Acid Surface Nanocrystals for Biocompatible Polysulfone Nanocomposites

Susana Anaya,[†] Berna Serrano,[†] Berta Herrero,[†,‡] Alberto Cervera,[§] and Juan Baselga*[,†]

[†]Department of Materials Science and Engineering and Chemical Engineering, Universidad Carlos III de Madrid, Avenida Universidad 30, 28911 Leganés, Madrid, Spain

[‡]Atria Science S.L, Avenida Gregorio Peces Barba 1, 28918 Leganés, Madrid, Spain

[§]Euroortodoncia S.L., Aeronáuticas 18-20, 28923 Alcorcón, Madrid, Spain

Supporting Information

ABSTRACT: High performance polysulfone/γ-alumina biocompatible nanocomposites are reported for the first time and the effects of γ-alumina surface modification are explored. We show that some fatty acids chemisorb over the surface of γ-alumina forming nanosized self-assembled structures. These structures present thermal transitions at high temperatures, 100 °C higher than the melting temperatures of the pure acids, and are further shifted about 50 °C in the presence of polysulfone. The chemistry involved in the chemisorption is mild and green meeting the stringent bio sanitary protocols for biocompatible devices. It has been found that the self-assembled structures increase mechanical strength by about 20% despite the foreseeable lack of strong particle−matrix interactions, which manifests as small variations in both the glass transition temperature and the Young's modulus. Electron microscopy observation of fractured surfaces has revealed that some acids induce an extended region of influence around the nanoparticles and this fact has been used to explain the enhancement of mechanical strength.

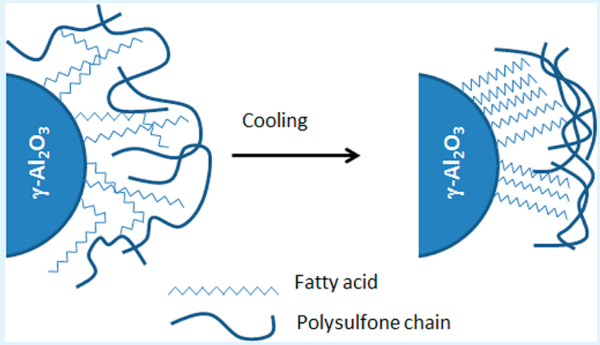

KEYWORDS: *nanocomposites, polysulfone, fatty acids, alumina*

1. INTRODUCTION

In addition to improving mechanical performance, a key requirement to develop polymer nanocomposites[1] for medical devices,[2] such as brackets or implants, is to meet stringent biosanitary protocols[3] throughout the nanocomposite fabrication process: from the biocompatible polymer and nanoparticle selection to the surface modification of nanoparticles, their dispersion and the final shaping processes. Among these, the surface modification step is particularly critical since it normally involves chemical reactants and solvents that are not explicitly accepted by regulators.[3] Nanocomposites for bioengineering applications, that is, that are in permanent contact with the body, are thus a separate class of nanocomposite materials for which a mild and specific surface chemistry needs to be developed.

The overall performance of polymer nanocomposites depends, among other factors, on the surface modification of the nanofillers[4] which has two main effects. On the one hand, it helps to stabilize nanoparticle dispersions and, on the other, it enhances miscibility and ensures a good interfacial contact with the polymer matrix. Concerning the first effect, most inorganic oxides used as nanofillers show a remarkable tendency to form aggregates due to the relatively strong van der Waals interactions associated with the presence of hydroxyl groups on their surface. Aggregates delay percolation and reduce the interphase volume fraction having thus a deleterious effect on both the mechanical and thermal properties.[5−14] Concerning the second effect, it is now accepted that a promising route consists of the functionalization of nanoparticles with polymer brushes with varying density and graft length.[15] However, the chemistry involved in such methods may not be adequate for biomedical applications.

To screen out particle−particle interactions several strategies have been explored and a detailed description of them can be found elsewhere.[16] Among these, chemisorption of long chain carboxylic acids onto the surface of inorganic nanoparticles through acid−base reactions may be of particular interest for the purposes of this work because of the mild character of their chemistry and the wide range of natural fatty acids that could be accepted as minor constituents.[3,17−20] The properties of their surface structure have been studied at the atomic level and it has been described that close to the isoelectric point these acids chemisorb forming insoluble carboxylates.[20−22]

Received: June 13, 2014
Accepted: July 27, 2014
Published: July 27, 2014

To the authors knowledge, nothing is known about the structure at higher scale lengths except for the early work of Allara and Nuzzo[23] who discovered that, above 11 carbon atoms, *n*-alkanoic acids physisorbed on an oxidized aluminum surface present closest packed structures with the same low surface free energy. Nothing is known also about the use of these acids as surface modifiers for advanced nanocomposites. Probably, the reason is associated with the foreseeable lack of strong particle−matrix interactions due to the low polarity of the alkanoic acid layer on the surface of the nanoparticles. Nevertheless, as we will show, chemisorption arrests the hydrocarbon chains in the monolayer providing adequate conditions for crystallization and these surface nanocrystals induce new mechanisms that enhance the strength of the nanocomposite.

In this paper we have selected polysulfone (PSF) as the matrix polymer. Its excellent thermal and mechanical properties along with its high temperature hydrolytic resistance and its biocompatibility,[24,25] make this polymer suitable for high-performance medical devices that require high temperature sterilization.[26,27] This polymer is currently used for brackets production but erosion induced by mastication may reduce its in-service life; thus, an increase of its strength is currently desired and may be achieved by dispersion of hard ceramic oxides, such as γ-alumina. This ceramic oxide was selected as nanoreinforcement since it shows minimal or no tissue reaction, blood compatibility tests are satisfactory[27,28] and its beneficial effects on mechanical properties have already been demonstrated.[9,29−32] Alumina particles will be surface modified with stearic, palmitic, erucic and oleic acids. Dry methods such as extrusion and microinjection will be used to prepare nanocomposites mimicking real industrial processing and allowing fabrication specimens with highly reproducible geometry. Except for the case of oleic acid, we will show that nanocrystals form over the surface of alumina presenting unusually high melting temperatures, around 170−190 °C and deeply modify the strength and fracture behavior of the nanocomposites despite the weak interfacial polymer−particle interactions.

2. MATERIALS AND METHODS

2.1. Materials. A commercially available polysulfone (PSF) Ultrason S2010 (Natural) of density 1.23 g·cm^{-3} was supplied by BASF. Characterization of the polymer (SEC) was done by Hoffman et al:[33] M_n = 13600, M_w = 53800.

γ-Al_2O_3 nanoparticles were purchased from Sigma-Aldrich with 50 nm nominal median size and 4 g·cm^{-3} density. Several long chain carboxylic acids, including two unsaturated acids, oleic and erucic, and two saturated acids, palmitic and stearic, were also purchased from Sigma-Aldrich; molecular formulas, molecular mass, and melting points are given in Supporting Information Table 1.

The solvents used to wash nanoparticles: ultrapure water and acetone (98%), as well as NaOH were purchased from Sigma-Aldrich Co, and they were used as received without further purification. No other chemicals were used in this work.

2.2. Characterization Techniques. Surface area was evaluated by nitrogen adsorption and desorption isotherm (Micromeritics New Gemini VII 2390 Series Surface Area Analyzers). Before determination, the samples were heated at 200 °C for more than 1 h to remove adsorbed water.

Thermogravimetric analysis (TGA), were performed with a PerkinElmer STA 6000 to study the chemisorption of carboxylic acids, the thermal stability of nanocomposites and to measure the final amount of nanoparticles in the nanocomposite. Conditions were: temperature range of 30−900 °C, heating rate 20 °C/min. An O_2 atmosphere was used to characterize surfactants on alumina particles. A N_2 atmosphere was used for PSF nanocomposites.

Fourier transform infrared spectroscopy (FTIR) was conducted with a PerkinElmer GX 2000 spectrometer in the medium range (4000−400 cm^{-1}) to test the physicochemical interaction between carboxylic acids and γ-alumina nanoparticles; resolution and number of scans were set to 1 cm^{-1} and 25 respectively.

Differential scanning calorimetry (DSC, PerkinElmer Pyris Diamond) was used to measure the glass transition temperature of the nanocomposites in the temperature range from 40 to 300 °C at a heating rate of 10 °C/min under nitrogen atmosphere.

Field emission scanning electron microscope (FESEM FEI Nova NANOSEM 230) was used to observe the dispersion state and effect of nanoparticles on the fracture of nanocomposite; samples were cryogenically fractured along the injection direction of bone specimens.

2.3. Surface Functionalization of γ-Alumina Nanoparticles. An already reported method for surface functionalization, based on the alkaline treatment of alumina, has been followed.[20] As received alumina had a specific surface of 138 m^2·g^{-1} but it is known that under alkaline conditions at pH = 11 alumina dissolves forming aluminate anions[34] with a relatively small equilibrium concentration (10^{-4} M), that is, the extent of the dissolution is limited to approximately 1%. To determine the effect of alkaline media on surface properties of alumina, as received alumina was treated for 1 h at pH = 11 and specific surface was measured again. Results are presented in Supporting Information Table 2 where it can be observed that specific surface only increases up to 150 m^2/g. Calculation of the amount of carboxylic acid needed for monolayer coverage was done taking this last value. Excess of carboxylic acid, that would require and extensive post-treatment washing step, was avoided. In a typical experiment 0.25−0.4 g of carboxylic acid were dissolved in 200 mL of an alkaline (NaOH) solution at pH ∼ 11 at 85 °C yielding a clear solution after 5 min; under these conditions, carboxylic acids were completely ionized. Immediately after, 1 g of alumina powder was added to the basic solution, vigorously stirred and sonicated in an ultrasonic bath for 60 min at 85 °C. After this time, the solution was cooled to room temperature, centrifuged at 4000 rpm for 15 min and filtered and washed several times with deionized water until neutral pH. Finally, the powder was washed several times with acetone to remove the physisorbed carboxylate while retaining the chemisorbed carboxylate surface coverage.[32] The final filtrated solid was dried in vacuum at 120 °C for at least 24 h. Alumina powders were analyzed by TGA to measure the amount of chemisorbed acid, $\Delta\omega$ (see Supporting Information Figure 1 and Table 1). Calculation of the surface density σ (molecules/nm^2) was done with the following expression $\sigma = \Delta\omega N_A 10^{18}/MS_p$, where M is the molar mass of the fatty acids and S_p is the specific surface of alumina particles. Particle density, ρ_P, was estimated using the following equation $\rho_P = (1 + \Delta\omega/\rho_{ac})]^{-1}$, where ρ_a and ρ_{ac} are the pure alumina (4 g·cm^{-3}) and fatty acid densities. Results were ρ_P(erucic) = 2.45 g·cm^{-3}; ρ_P(stearic) = 2.69 g·cm^{-3}; ρ_P(oleic) = 2.75 g·cm^{-3}; ρ_P(palmitic) = 3.06 g·cm^{-3}.

2.4. Nanocomposite Fabrication. Incorporation of γ-alumina in the polysulfone matrix was carried out using a HAAKE Minilab micro compounder equipped with a conical counter-rotating silicon carbide hardened twin screw extruder. Neat PSF was mechanically mixed with γ-alumina nanoparticles and the premix was dried at 140 °C for 24 h to remove moisture before compounding. After a preliminary rheological study it was concluded that the best processing conditions were: barrel temperature 360 °C, recirculation time 10 min and screw rotating speed 150 rpm. A 10% w/w master batch was initially prepared with modified and unmodified nanoparticles and the molten polymer strand was quenched at room temperature and pelletized. Samples containing 1−5% w/w nanoparticles were prepared by dilution with fresh PSF pellets and pelletized as well. Maximum loading was set at 5% since higher loadings resulted in nonhomogeneous samples. The resulting nanocomposites were homogeneous but light yellow colored. Yellowing increased with the amount of γ-alumina and notably decreased when surface modified particles were used, except for the case of oleic acid.

The extruded pellets of neat PSF and each set of the different compositions were molded using a Battenfeld Microsystem 50 micro molding machine; molding conditions were: mold temperature 135 °C, barrel temperature 350 °C, die temperature 345 °C, injection speed 500 mm·s^{-1}, injection pressure 989 bar, cycle time: 20 s. A mold specifically designed for this work was used to fabricate mini specimens with adequate geometry for tensile testing as shown in Supporting Information Figure 2. Before testing, all specimens were aged at 140 °C and 50% relative humidity for 24 h to remove residual stresses.

Highly loaded composites (50%) were prepared for analyzing the thermal behavior of the alkanoic acid monolayers. They could not be prepared by injection molding due to their extremely high viscosity so a solvent casting method with *N*-methylpyrrolidone was used instead. After an exhaustive vacuum drying process, the cast solid was hot pressed at 360 °C (Fontijne LabPro 400) for 10 min to eliminate any remaining solvent and then quickly cooled down to room temperature using the air/water system of the platen press.

2.5. Mechanical Measurements. Tensile testing was performed according to UNE-EN ISO 527-2 standard in a Shimadzu Autograph-1KN testing machine. The crosshead speed was set to 1 mm/min consistent with the standard and tests were done under the assumption of plane stress conditions. The mini-bone shaped specimens (16 × 3 × 1 mm^3) were prepared as described in the nanocomposite fabrication section. The average value of the Young modulus, tensile strength and strain at failure for each composition was obtained from five independent measurements. In some samples, optical clarity was visually monitored during the test and the stress at which whitening appeared was recorded.

3. RESULTS AND DISCUSSION

3.1. Chemisorption of Long Chain Fatty Acids. To confirm chemisorption of long chain fatty acids on γ-Al_2O_3 and to study their interaction, modified nanoparticles were studied by Fourier transformed spectroscopy (FTIR) and thermogravimetry. Regions of interest of the FTIR spectra of neat and surface treated γ-alumina nanoparticles as well as band assignment are shown in Figure 1. For comparison purposes, FTIR spectra of pure carboxylic acids are presented in the Supporting Information Figure S1.

Neat alumina presents a small absorption at around 1630 cm^{-1} that can be assigned to surface species with Dawsonite-like structure which may be formed by adsorption[35] of H_2O and CO_2. Asymmetric and the symmetric CH_2 stretching bands appear at 2920−2850 cm^{-1}. Vinyl band (=CH−) of unsaturated fatty acids appears at around 3000 cm^{-1}. Carbonyl band (C=O) of free carboxylic acid groups (~1700 cm^{-1}) is absent (Supporting Information Figure S1), in accord with TGA results. The new band at 1590−1560 cm^{-1} is assigned to asymmetric stretching of the carboxylate group (COO^-)[22,36] and clearly indicates that a new compound of aluminum carboxylate has been formed. Vibrational deformation of methylenic groups adjacent to the carboxylate[37] appears at ~1467 cm^{-1} and symmetric stretching of carboxylate[22] appears at 1410 cm^{-1}.

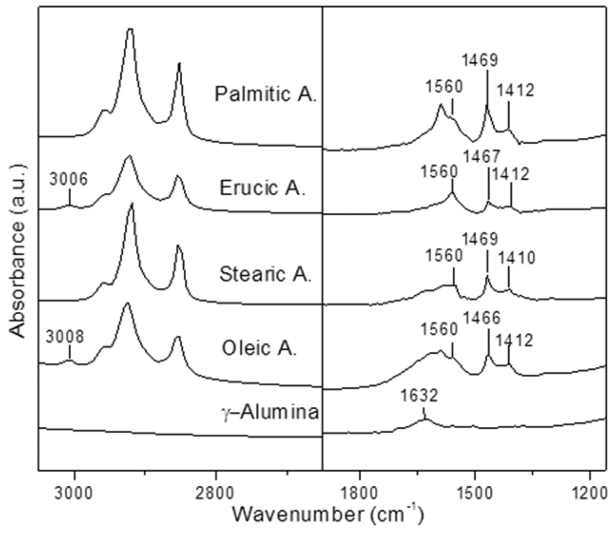

Figure 1. High (left) and low energy (right) Fourier transform infrared (FTIR) spectra of as-received and functionalized γ-alumina.

Interactions between carboxylate and metal atoms have been classified as monodentate, bidentate, bridging bidentate, and ionic interaction.[21,22,38] The relative wavenumber separation, Δ, between the asymmetric and symmetric carboxylate stretching bands, appearing at ~1560 cm^{-1} and ~1410 cm^{-1} respectively, or 1590 and 1467 cm^{-1}, can be used to distinguish these interactions[21]. Figure 1 reveals that Δ is approximately constant for all studied acids with a value of ~150 cm^{-1}, suggesting that the representative interaction between the COO^- group and the Al^{3+} ion corresponds to a bridging binuclear bond.

Thermogravimetric analysis (TGA) was performed on all samples to measure the surface density of chemisorbed carboxylates on γ-Al_2O_3 surface. Representative behavior is shown in Supporting Information Figure S2 and the calculated surface density of the fatty acids is presented in Table 1. Surface density data range between 1.5 and 2.5 molecules·nm^{-2} (1.1 × 10^4 − 2.4 × 10^4 grafts per particle) which is in fair accordance with the bridging bidentate bonding revealed by FTIR.

Table 1. Thermogravimetric Analysis of Nanoparticles Coated with Natural Fatty Acids

	weight loss peak (°C)	Δ*w* (900 °C) (%)	surface density (molecules/nm^2)
γ-Al_2O_3/oleic	445	15	2.3
γ-Al_2O_3/ stearic	450	15	2.1
γ-Al_2O_3/ palmitic	462	9	1.5
γ-Al_2O_3/ erucic	460	21	2.5

3.2. Characterization of Nanocomposites. The lack of strong interactions between the low polarity surface of coated alumina and PSF manifests as negligible variations in both the relaxational behavior and thermal resistance of the nanocomposites (see Supporting Information Table 3 and Supporting Information Figure S4). Concerning the glass transition temperature, T_g, it does not appreciably change with respect to neat PSF (190 °C) irrespective of the loading content or surface modifier. In addition, the width of the transition, as measured by the difference between the temperatures at start and end of the relaxation, and the strength of the transition, as measured by the change in heat capacity, also remain constant: $\Delta T = 29 \pm 1$ K and $\Delta C_p = 0.29 \pm 0.02$ J·g^{-1}·K^{-1} respectively.

The absence of measurable effects of nanoparticles on T_g in PSF is not uncommon. It has been found in several PSF nanocomposites loaded with carbon nanotubes,[39,40] polyhedral oligomeric silsesquioxane[41] and organosilicates[42] although other similar systems present opposite behavior. An example is poly(methyl methacrylate)(PMMA)/γ-Al_2O_3, a deeply

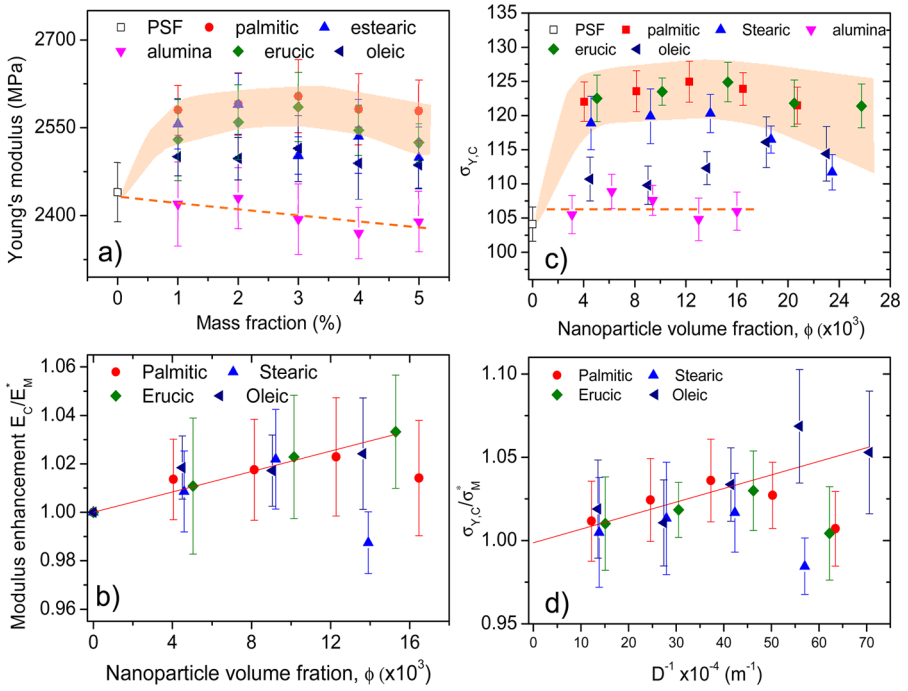

Figure 2. (a) Young's moduli of the nanocomposites as a function of nanoparticle mass fraction; shaded envelope corresponds to systems for which a noticeable enhancement has been found (stearic, erucic and palmitic); dotted line is a guide for the eye and shows data trends for neat alumina. (b) Modulus enhancement factor as a function of nanoparticle volume fraction. Error bars correspond to the standard deviation of five independent measurements. Straight line corresponds to the fitting of data to a modified Halpin–Tsai equation (see Supporting Information Annex, eq 5). (c) Yield stress of the nanocomposites as a function of nanoparticle volume fraction; shaded envelope corresponds to systems for which an enhancement has been found (stearic, erucic and palmitic); dotted line is a guide for the eye and shows data trends for neat alumina. (d) Yield stress enhancement factor as a function of interparticle distance (see text for details); error bars correspond to the standard deviation of five independent measurements; straight line corresponds to the fitting of data to eq 1

studied system[9,29] representative of the *confinement effect*[43−46,45−48] due to the weak polymer–particle interactions. In this system the polymer at the interfacial region has an enhanced mobility that substantially reduces the *Tg* of the composite and changes its tensile behavior from fragile to ductile fracture.

PSF and PMMA are conformationally flexible polymers ($C_{\infty,PSF}$ = 2,[47,48] $C_{\infty,PMMA}$ = 8.1[49]) that should interact with alumina in a similar way according to their similar surface tension[49] ($\gamma_{20°,PSF}$ = 46.6 mN/m, $\gamma_{20°,PMMA}$ = 41.1 mN/m) and cohesive energy density values[49] (δ_{PSF} = 20.3 MPa$^{1/2}$, δ_{PMMA} = 22.7 MPa$^{1/2}$). Therefore, their different behavior must be probably associated with their very different structure in the amorphous state, as revealed by their entanglement density values,[48] ν_e, which may be the ultimate responsible for their very different *Tg* and mechanical properties. ν_e for PSF (5.5 × 10^{-4} mol/cm^3) is four times larger than for PMMA (1.3 × 10^{-4} mol/cm^3) and, as pointed out by Mills,[50] this entanglement network is maintained in the glassy state when cooled from the melt. Therefore, we hypothesize that the segmental mobility in PSF must be so severely constrained that the reduction in entanglement density by the presence of the interface, the so-called *confinement effect*, must be limited to a region near the surface too small to cause any effect on the bulk polymer relaxational behavior. Literature on alumina nanocomposites with other high performance polymers is scarce but in a recent work[30] it is also reported a lack of variation of the T_g of polycarbonate when it is blended with the neat inorganic filler. For polycarbonate ν_e is even higher than for PSF (6.7 × 10^{-4} mol/cm^3) and this is in accordance with our assumption.

3.3. Young's Modulus and Strength. However, coated nanoparticles have a deep effect on mechanical behavior of nanocomposites as studied by tensile testing. Representative engineering stress–strain curves are shown in Supporting Information Figure S5. In Figure 2a, composite Young's modulus, E_C, is plotted as a function of nanoparticle mass fraction for all systems.

Although data scattering appears to be high, relative errors range between 1.6% and 2.5%, which are more than acceptable considering typical uncertainty in this kind of measurements. Except for the case of neat alumina, all systems using surface modified alumina show an increased value of E_C up to a maximum at about 3% (w/w), particularly for erucic, palmitic and stearic systems. This is a common behavior found in many filled systems usually attributed to cluster formation. However, the great jump found at low loadings cannot be accounted for with known micromechanical models. For particulate filled polymers with weak interfacial interactions the lower bound shear modulus enhancement micromechanical model[51] should apply (see Supporting Information Annex). According to this model, the maximum increment of E_C for a representative system (2% palmitic) should be 1.6%, while the experimental enhancement is 6.2%, three times higher.

We attribute this discrepancy to chain orientation in the injection process. The micromechanical models for particulate composites use the matrix as the reference phase and calculate the enhancement factor by the sole presence of uniformly dispersed particles. The underlying assumption is that the properties of the isotropic matrix must be the same in both the pure state and in the composite. When composites are prepared

by injection molding, this requirement may not be fulfilled because of the flow perturbations of the melt induced by the presence of nanoparticles. Some rheological studies on the flow of melts loaded with spherical and cylindrical nanoparticles[52,53] show dramatic changes in the flow field in the converging flow region at the entrance zone of the capillary die, which is geometrically equivalent to the gate entrance in an injection mold. In particular, a vortex enhancement was found which resulted in the enlargement of the acceleration zone and the increase of the fluid velocity. In turn, this increased the strength of the elongational field and the elongational stress at the entrance of capillary. We hypothesize that under our processing conditions (volume, temperature and time), the elongated melt would quickly cool and retain at least to some extent the melt orientation. As a consequence, Young's modulus would be slightly higher than in the absence of particles and fracture deformation would be lower and that is already observed in the mechanical tests (see Supporting Information Figure S5).

Having these ideas in mind, the reference state for nanocomposites loaded with nanoparticles should correspond to pure neat polysulfone subjected to the same extensional flow than a loaded one. Obviously, this is not easy to achieve experimentally but an iterative method to estimate it can be inferred. A detailed explanation is given in Supporting Information Annex. Using this method, the true normalization constant E_M^* was calculated for all the systems and its average value was E_M^* = 2510 ± 40 MPa, 3% higher than the value measured for polysulfone. Although this variation is small in absolute terms, it is important to consider it to properly analyze experimental data. The true enhancement factor is presented in Figure 2**b**. To confirm the validity of the present analysis the results have been analyzed using eq 1, which is valid for diluted suspensions.

$$\lim_{\phi \to \infty} \frac{E_C}{E_M^*} = 1 + A\phi \tag{1}$$

Coefficient A, which depends on the shear modulus of the polymer matrix and of the alumina particles as well as on the Poisson coefficient of the matrix (see Supporting Information Annex), has the well-known value of 5/2 for perfectly rigid particles suspended in an incompressible matrix; for our system, the theoretical value is 2.26. The initial linear section of the data shown in Figure 2 (bottom left), up to ϕ = 0.016 excluding the neat alumina, was fitted to eq 1 and the recovered slope was 2.11 ± 0.12, which is in good agreement with the theoretical result and confirms that (i) mechanical behavior of pure matrix polymer can no longer be used as the reference to correctly analyze mechanical behavior of nanocomposites if these are obtained by injection molding; (ii) reinforcement can be explained, as expected, in terms of the lower bound micromechanical model; (iii) there is almost no adhesion between the particles and the matrix.

Nevertheless, despite the lack of adhesion, strength analysis reveals that the interfacial zone is able to effectively transfer stresses across it. The strength of composites results from a balance of two opposing effects: particles act as stress concentrators or as barriers to crack growth. It is commonly observed that in the case of no adhesion between the particles and the matrix, the first effect predominates and strength usually decreases.[54] But, as shown in Figure 2c, yield stress increases with particle content suggesting that the second effect operates. From this figure it becomes also clear that the strength of neat alumina and oleic systems is lower than for palmitic, erucic or stearic systems, in accord with the observed earlier whitening during loading in the stress−strain tests (see Supporting Information Figure 5) for these systems.

As with Young's modulus, the maximum yield stress is also achieved for the palmitic system with a notably higher relative increment, around 20%, while the strength of nanocomposites loaded with neat alumina remains approximately constant. Coherently with the analysis of Young's modulus data, a different reference state should be considered also for yield stress. Among the models commonly used to explain strength in particulate composites, that of Young and Beaumont[54,55] allows comparing different systems. According to this phenomenological model, the yield stress of a composite is a function of the interparticle distance D, as shown in eq 2

$$\sigma_C = \sigma_M + \frac{S}{D} \tag{2}$$

where D can be calculated from the primary particle diameter d_P and the particle volume fraction ϕ, according to[54] $D = 2d_P(1 - \phi)/3\phi$; S is a constant that depends on the interfacial adhesion. Fitting of σ_C in the range $0 \le \phi \le 0.02$ as a function of D^{-1} has been used to extract the yield stress of the reference matrix, σ_M^*. Its average value was σ_M^* = 117 ± 6 MPa, which is 13% higher than the neat PSF yield stress measured value, which was σ_M = 104 ± 3 MPa. The relative increment of yield stress, given by the quotient σ_C/σ_M^* is plotted against D^{-1} in Figure 2d; fitting to eq 2 gives a straight line with slope $S = (9.5 \pm 0.5)\cdot 10^{-6}$ MPa·m. As expected, this value is smaller than other published data in which adhesion among particles and matrix is stronger as the case of epoxy filled with silane treated glass.[55]

3.4. Fracture Behavior and Nanocrystals Formation. A possible origin of the different behavior of neat alumina/oleic and palmitic/erucic/stearic systems can be understood observing the morphology of fracture surfaces. Two different surfaces were analyzed: fragile fracture surfaces, prepared quickly breaking samples that were frozen in liquid N_2, and ductile fracture surfaces, prepared from samples loaded to failure in the testing machine.

Fragile fracture surfaces of the neat alumina and oleic systems are very similar; a representative image is shown in Figure 3a, where particles appear to be uniformly dispersed and surrounded by plastically deformed polymer in a buttonhole fashion with diameter less than a micron, without particle−matrix connectivity; the lack of connectivity with the matrix indicates a bad interfacial contact probably because of the reactivity of alumina. γ-Al_2O_3 has a highly reactive surface and close to its isoelectric point the neutral surface hydroxyl groups are active as radical generators as it has been deduced from studies on the catalytic activity of γ-Al_2O_3 in the degradation of some colorants.[56] At the high temperatures involved in composite processing, alumina may induce chemical degradation of the polymer, probably through chain scission. As a consequence, polymer−particle contact becomes poorer degrading thus its mechanical performance.

This bad contact also manifests in the ductile fracture surfaces (Figure 3d and e) where a region with a morphology resembling viscous flow where torn particles leave relatively large wakes as they move or even holes if they become detached from the matrix can be observed. In the absence of any surface treatment (Figure 3d) stopped crazes have been found very close to the edge of the specimen; very large fibrils

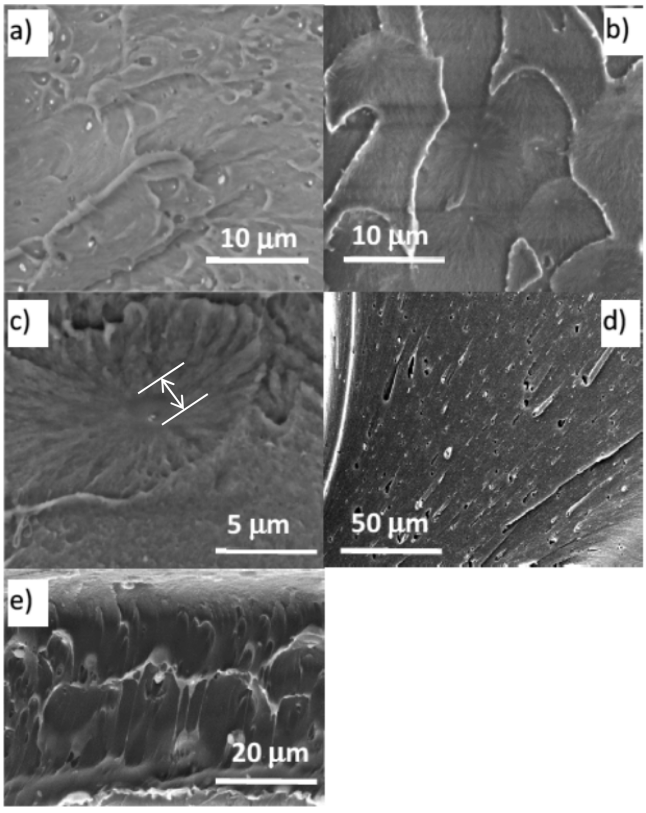

Figure 3. Fracture surface FESEM micrographs: (a, b, and c) fragile fractures and (d and e) ductile fractures. (a) PSF/γ-Al_2O_3 3%. (b) PSF/γ-Al_2O_3–palmitic 3%. (c) Same as that in panel b but at higher magnification; the arrow shows the region of influence of the particle. (d) Frontal view PSF/γ-Al_2O_3–oleic 3%. (e) Frontal view PSF/γ-Al_2O_3. Stress direction in micrographs d and e is perpendicular to the images.

several microns long can be clearly observed alongside, with detached aggregates identified within the holes of the fibrils.

A representative image of the fracture surface for alumina treated with the other fatty acids is presented in Figure 3b. Along with hackle or mackerel bands, the most interesting feature of this image is the presence of parabolic markings in the center of which a nanoparticle or aggregate is located. Figure 3c corresponds to a magnified image of this feature and reveals a coarse surface at the sides of the parabola, plenty of prominences and channels, which may indicate rapid crack propagation, in accordance with previous findings.[50] However, the surface becomes smooth in the region around the focus, just where the particle is located as indicated by the arrow inserted in the image. It seems therefore that the crack slows down in a region around 1 μm in diameter near the particles indicating a good interfacial contact in accord with the higher yield stress observed for these systems. The very different behavior shown by these acids with respect to oleic system must be related to the different structure of these acids in the monolayer. Since chemisorption immobilizes the hydrocarbon chains over the alumina surface, nanosized crystals could be formed during nanocomposite processing.

XRD is of the paramount importance for characterizing crystalline nanostructures. However, alumina particles present a very intense line just below 10°, which precludes the use of diffractions at low angles for identification, and a small and broad line at 20°, which is coincident with diffraction lines of some fatty acids (see Supporting Information Figure 6). Considering that the amount of fatty acids on the surface of nanoparticles is small and not all may form part of crystalline nanostructures (see discussion below), diffractions of fatty acids on the surface are completely obscured by the intense diffractions of the highly crystalline alumina substrate. As a consequence, it seems difficult to unambiguously ascertain the crystalline structure of the nanostructures by XRD.

Alternatively, to verify if nanocrystals were formed two different set of experiments were done. In the first one, surface treated nanoparticles were investigated by DSC. In the second one, it was checked whether crystals could also be formed in the presence of the PSF matrix. The results of the first experiment are presented in Figure 4a. Alumina nanoparticles treated with palmitic and erucic acids presented two clear endotherms at around 126 and 147 °C and those treated with stearic acid presented a single endotherm at 125 °C. The total enthalpy associated with these endotherms was ~6 J/g for palmitic acid and ~3 J/g for both erucic and stearic acids. These values are extremely low in comparison with the melting enthalpies of the pure substances but it is interesting to observe

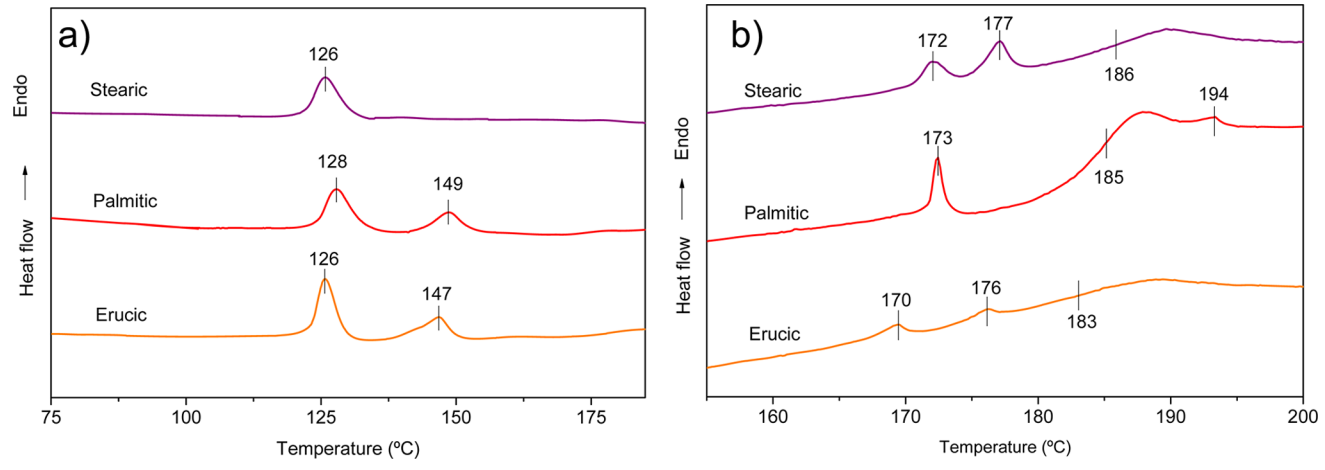

Figure 4. Second scan DSC runs after cooling at 40 °C/min for (a) alumina modified with erucic, palmitic, oleic and stearic acids and (b) for a 50% (w/w) nanocomposite with alumina particles modified with erucic, stearic and palmitic acids. Vertical lines show the temperatures for the several endotherms and the glass transition of the polymer at 183–186 °C. A shift of about 45 °C is observed in the presence of polysulfone matrix.

that endotherm temperatures are shifted about 50−100 °C with respect to the melting points of the pure substances (see Supporting Information Table 1). Thermogrammes of oleic treated nanoparticles did not present any melting even at the sub ambient temperature range. These results confirm that the long chain fatty acids can form nanocrystals over the surface of γ-alumina with the exception of oleic acid.

For the second experiment it was necessary to prepare highly loaded composites (see Experimental) since the mass fractions of fatty acids were too small to be detected with our instrument. Results for the second scan after cooling at −40 °C/min are presented in Figure 4b. Two clear endotherms are observed for erucic and stearic systems appearing at 171 and 176 °C, before the glass transition of the polymer which is 4 °C below the bulk Tg of PSF. For palmitic an endotherm clearly appears also at 172 °C, before Tg of the matrix, but a second small endotherm was detected above the Tg of the matrix, at 194 °C. Neither did oleic systems present any melting in the measured temperature range. The total enthalpy associated with these endotherms was reduced with respect to the treated nanoparticles, being ∼4 J/g for palmitic acid, ∼1 J/g for erucic acid and 3 J/g for stearic acid. Endotherm temperatures in the composite were further shifted about 50 °C to higher temperatures with respect to the particles without PSF.

To the author's knowledge, this is the first time surface self-assembled structure formation is reported. In qualitative terms, the high transition temperatures observed in the absence and in the presence of PSF, may find an explanation in successive entropic reductions assuming that phase transition enthalpy does not change very much for a given allotrope. The first reduction in phase transition entropy may be associated with the immobilization of the fatty acid chains over the surface of nanoparticles, which eliminates the translational degree of freedom. This fact suggests that the term "melting" may be inadequate.

The fact that stearic crystals present a single endotherm in the nanoparticles but two endotherms in the composite indicates that PSF chains at the interface somehow influence the crystallization process. Thus, we might speculate that on cooling, PSF segments may be so close to the fatty acid chains during its transition so as to reduce the number of possible microstates during the phase transition; this phenomenon further reduces the phase transition entropy increasing the transition temperature.

However, an alternative explanation may be given in terms of the autophobic effect or dewetting[5,57−60] which might operate by virtue of the high graft density, the high molecular weight of the polymer matrix in comparison with the molecular weight of the fatty acids, and the unfavorable interactions between PSF and the hydrocarbon grafts. The experimental fact that phase transition occurs close to the Tg of the polymer, a temperature range at which the polymer relaxation time is longer than the characteristic relaxation time for phase transitions of small molecules, suggests that either polymer exclusion from the crystals or dewetting may occur, and both may leave the polymer in a compressed state in a region close to the fatty acid monolayer. This plausible fact may be the origin of the extended region of influence observed in Figure 3c, and, consequently, of the observed increased strength of the composites.

Nevertheless, it remains as a question to be answered why oleic acid does not crystallize.

As mentioned above, pristine γ-Al_2O_3 is involved in the local generation of chromophoric groups associated with polymer chain scission at the high processing temperatures used in this work and this fact is the main reason for the strong coloring found when using neat alumina or alumina modified with oleic acid. But when γ-Al_2O_3 is surface modified with palmitic, erucic and stearic fatty acids, PSF degradation becomes greatly reduced. Considering DSC results we can speculate that the presence of a coating layer of nonpolar palmitic, stearic or erucic acids distances and protects the matrix polymer from the generation of radicals from γ-Al_2O_3. In the case of oleic acid, we currently think that alumina may degrade this unsaturated acid at the high temperatures used for preparing the samples preventing its crystallization.

Which kind of crystalline structure is formed at the interface and which solid−solid phase transitions operate, the reasons for such low enthalpy values, the origin of the two endotherms and the influence of the polymer matrix on their appearance or disappearance are some open questions that have not been answered hitherto in the checked literature on nanocomposites and require further research that is presently being carried out. However, in our opinion, the important point here is that even in the presence of the polymer, alkanoic monolayers crystallize at temperatures very near the T_g of the matrix. Thus, the existence of a solid-like interfacial region formed during the cooling of the composites is confirmed for palmitic, erucic and stearic systems and not for the oleic case, and this contributes to increase the strength of the nanocomposites.

4. CONCLUSIONS

Oleic, palmitic, erucic, and stearic fatty acids have been chemisorbed onto the surface of γ-alumina nanoparticles via bridging bidentate complex formation. Surface treated alumina has been dispersed in polysulfone by extrusion and nanocomposites with varying amounts of the nanofiller have been prepared by injection molding. Glass transition temperatures were measured for all the nanocomposites and almost no variation was observed, contrary to what was observed for PMMA/γ-alumina nanocomposites. This fact was attributed to the very high entanglement density of PSF in comparison with PMMA. Young modulus results have been analyzed in terms of the lower bound shear modulus enhancement micromechanical model. It has been shown that it is not possible to fit data if a new reference state is not postulated. The existence of this reference state can be explained considering an extra chain orientation during injection molding in the presence of γ-alumina nanoparticles. Strength results show a noticeable improvement of about 20% for the palmitic system. Analysis of the fracture surfaces has revealed the existence of an extended region of influence for this system of about 1 μm around the nanoparticles. The origin of this region has been explored by DSC and it has been found that with the only exception of oleic acid, fatty acids self-assemble giving nanostructures on the surface of the γ-alumina nanoparticles that present single or dual endotherms shifted 145 °C above the normal melting points of the pure acids. The temperature ranges of these endotherms and of the glass transition of polysulfone are coincident suggesting that, on cooling, polymer exclusion from the crystals or dewetting may occur leaving the polymer in a compressed state in a region close to the fatty acid monolayer. This plausible fact may be the origin of the observed extended region of influence and, consequently, of the observed

increased strength of the composites despite de foreseeable lack of strong particle−matrix interactions.

■ ASSOCIATED CONTENT

Supporting Information

Chemical characteristics of long chain carboxylic acids used as surface modifiers, surface properties of γ-alumina before and after 1 h at pH = 11, glass transition temperatures of PSF nanocomposites, FTIR bands of the four studied acids in both the pure state and reacted with alumina particles, representative TGA thermogram of neat γ-alumina and modified with palmitic acid and the corresponding weight loss derivative, dimensions of the molded mini specimens (in mm), digital photos of the Polymer Composite Group logo printed below specimens to demonstrate their transparency, TGA thermograms of neat PSF, PSF loaded with 5% unmodified γalumina and PSF loaded 5% γ-alumina modified with the fatty acids indicated in the inset, representative engineering stress−strain curves for neat PSF, PSF loaded with 3% neat alumina and PSF loaded with 3% modified alumina, XRD patterns of fatty acids, neat alumina and modified alumina, method for retrieving the Youngs modulus of the true reference state. This material is available free of charge via the Internet at http://pubs.acs.org/

■ AUTHOR INFORMATION

Corresponding Author

*Fax: 34916249430. Tel: 34916249467. E-mail: jbaselga@ing.uc3m.es.

Notes

The authors declare the following competing financial interest(s): we have applied for the patent S. Anaya, B. Serrano, J. Baselga, A. Cervera, I. Garca, PCT/ES2013/070243, April 4th 2013.

■ ACKNOWLEDGMENTS

This work was supported by granst Nanomod (MAT2010-17091) from the Spanish Ministerio de Economía y Competitividad and NANOBRAK (04-AEC0810-000056/2008), as well as to the INTERFASES consortium (Comunidad Autónoma de Madrid, Spain).

■ REFERENCES

(1) Balazs, A. C.; Emrick, T.; Russell, T. P. Nanoparticle Polymer Composites: Where Two Small Worlds Meet. *Science* **2006**, *314*, 1107−1110.
(2) Xia, Y. Nanomaterials at Work in Biomedical Research. *Nat. Mater.* **2008**, *7*, 758−760.
(3) Commission Regulation (EU) No 10/2011 of 14 January 2011 on Plastic Materials and Articles Intended to Come into Contact with Food. *Off. J. Eur. Union* **2011**, *54*, L12/1−L12/89.
(4) Schadler, L. Nanocomposites: Model Interfaces. *Nat. Mater.* **2007**, *6*, 257−258.
(5) Qiao, R.; Deng, H.; Putz, K. W.; Brinson, L. C. Effect of Particle Agglomeration and Interphase on the Glass Transition Temperature of Polymer Nanocomposites. *J. Polym. Sci., Part B: Polym. Phys.* **2011**, *49*, 740−748.
(6) Chae, D. W.; Kim, B. C. Characterization on Polystyrene/zinc Oxide Nanocomposites Prepared from Solution Mixing. *Polym. Adv. Technol.* **2005**, *16*, 846−850.
(7) Ciprari, D.; Jacob, K.; Tannenbaum, R. Characterization of Polymer Nanocomposite Interphase and Its Impact on Mechanical Properties. *Macromolecules* **2006**, *39*, 6565−6573.
(8) Han, K.; Muhuo, Y. Study of the Preparation and Properties of UV-Blocking Fabrics of a PET/TiO2 Nanocomposite Prepared by in Situ Polycondensation. *J. Appl. Polym. Sci.* **2006**, *100*, 1588−1593.
(9) Ash, B. J.; Siegel, R. W.; Schadler, L. S. Mechanical Behavior of Alumina/Poly (Methyl Methacrylate) Nanocomposites. *Macromolecules* **2004**, *37*, 1358−1369.
(10) Bolhuis, P.; Louis, a.; Hansen, J.-P. Influence of Polymer-Excluded Volume on the Phase-Behavior of Colloid−Polymer Mixtures. *Phys. Rev. Lett.* **2002**, *89*, 128302.
(11) Kovačević, V.; Lučić, S.; Leskovac, M. Morphology and Failure in Nanocomposites. Part I: Structural and Mechanical Properties. *J. Adhes. Sci. Technol.* **2002**, *16*, 1343−1365.
(12) Kovačević, V.; Leskovac, M.; Lučić Blagojević, S. Morphology and Failure in Nanocomposites. Part II: Surface Investigation. *J. Adhes. Sci. Technol.* **2002**, *16*, 1915−1929.
(13) Tannenbaum, R.; Zubris, M.; David, K.; Ciprari, D.; Jacob, K.; Jasiuk, I.; Dan, N. FTIR Characterization of the Reactive Interface of Cobalt Oxide Nanoparticles Embedded in Polymeric Matrices. *J. Phys. Chem. B* **2006**, *110*, 2227−2232.
(14) Husain, S.; Koros, W. J. A General Strategy for Adhesion Enhancement in Polymeric Composites by Formation of Nano-structured Particle Surfaces. *J. Phys. Chem. C* **2007**, *111*, 652−657.
(15) Meng, D.; Kumar, S. K.; Lane, D.; Grest, J. M.; Effective, G. S. Interactions Between Grafted Nanoparticles in a Polymer Matrix. *Soft Matter* **2012**, *8*, 5002.
(16) Faure, B.; Salazar-Alvarez, G.; Ahniyaz, A.; Villaluenga, I.; Berriozabal, G.; De Miguel, Y. R.; Bergström, L. Dispersion and Surface Functionalization of Oxide Nanoparticles for Transparent Photocatalytic and UV-Protecting Coatings and Sunscreens. *Sci. Technol. Adv. Mater.* **2013**, *14*, 023001.
(17) Chen, L.; Xu, J.; Holmes, J. D.; Morris, M. a. A Facile Route to ZnO Nanoparticle Superlattices: Synthesis, Functionalization, and Self-Assembly. *J. Phys. Chem. C* **2010**, *114*, 2003−2011.
(18) Leite, E. R.; Ribeiro, C. Trends and Perspectives in Nanoparticles Synthesis. In *Crystallization and Growth of Colloidal Nanocrystals*; Springer: New York, 2012; pp 83−92.
(19) Comparelli, R.; Fanizza, E.; Curri, M.; Cozzoli, P.; Mascolo, G.; Passino, R. Agostiano, a. Photocatalytic Degradation of Azo Dyes by Organic-Capped Anatase TiO Nanocrystals Immobilized onto Substrates. *Appl. Catal., B* **2005**, *55*, 81−91.
(20) Liu, J.-C.; Jean, J.-H.; Li, C.-C. Dispersion of Nano-Sized Gamma-Alumina Powder in Non-Polar Solvents. *J. Am. Ceram. Soc.* **2006**, *89*, 882−887.
(21) Capelle, H. a.; Britcher, L. G.; Morris, G. E. Sodium Stearate Adsorption onto Titania Pigment. *J. Colloid Interface Sci.* **2003**, *268*, 293−300.
(22) Wu, N.; Fu, L.; Su, M.; Aslam, M.; Wong, K. C.; Dravid, V. P. Interaction of Fatty Acid Monolayers with Cobalt Nanoparticles. *Nano Lett.* **2004**, *4*, 383−386.
(23) Allara, D. L.; Nuzzo, R. G. Spontaneously Organized Molecular Assemblies. 1. Formation, Dynamics, and Physical Properties of n-alkanoic acids adsorbed from solution on an oxidized aluminum surface. *Langmuir* **1985**, *1*, 45−52.
(24) Wenz, L. M.; Merritt, K.; Brown, S. A.; Moet, A.; Steffee, A. D. In Vitro Biocompatibility of Polyetheretherketone and Polysulfone Composites. *J. Biomed. Mater. Res.* **1990**, *24*, 207−215.
(25) El-Hibri, M. J.; Weinberg, S. A. Polysulfones. In *Encyclopedia of Polymer Science and Technology*; John Wiley & Sons, Inc.: Hoboken, NJ, 2002.
(26) Clark, W. R.; Gao, D. Properties of Membranes Used for Hemodialysis Therapy. *Semin Dial* **2002**, *15*, 191−195.
(27) Thamaraiselvi, T. V.; Rajeswari, S. Biological Evaluation of Bioceramic Materials - A Review. *Trends Biomater. Artif. Organs* **2004**, *18*, 9−17.
(28) Christel, P. S. Biocompatibility of Surgical-Grade Dense Polycrystalline Alumina. *Clin. Orthop. Relat. Res.* **1992**, *282*, 10−18.
(29) Ash, B. J.; Siegel, R. W.; Schadler, L. S. Glass-Transition Temperature Behavior of alumina/PMMA Nanocomposites. *J. Polym. Sci., Part B: Polym. Phys.* **2004**, *42*, 4371−4383.

(30) Hakimelahi, H. R.; Hu, L.; Rupp, B. B.; Coleman, M. R. Synthesis and Characterization of Transparent Alumina Reinforced Polycarbonate Nanocomposite. *Polymer* **2010**, *51*, 2494−2502.
(31) Sawyer, W. G.; Freudenberg, K. D.; Bhimaraj, P.; Schadler, L. S. A Study on the Friction and Wear Behavior of PTFE Filled with Alumina Nanoparticles. *Wear* **2003**, *254*, 573−580.
(32) Guo, Z.; Pereira, T.; Choi, O.; Wang, Y.; Hahn, H. T. Surface Functionalized Alumina Nanoparticle Filled Polymeric Nanocomposites with Enhanced Mechanical Properties. *J. Mater. Chem.* **2006**, *16*, 2800−2808.
(33) Hoffmann, T.; Pospiech, D.; Kretzschmar, B.; Reuter, U.; Häußler, L.; Eckert, F.; Perez-Graterol, R.; Sandler, J. K. W.; Altstädt, V. Modification of Polysulfones by Carboxylic Acids. *High Perform. Polym.* **2007**, *19*, 48−61.
(34) Pourbaix, M. *Atlas of Electrochemical Equilibtia in Aqueous Solutions*; NACE: Houston, TX, 1974; p 171.
(35) Lee, D. H.; C, R. A., Sr. An FTIR Spectral Investigation of the Structural Species Found on Alumina Surfaces. *Mater. Lett.* **1995**, *23*, 241−246.
(36) Kumar, T. V. V; Prabhakar, S.; Raju, G. B. Adsorption of Oleic Acid at Sillimanite/water Interface. *J. Colloid Interface Sci.* **2002**, *247*, 275−281.
(37) Lee, S. J.; Han, S. W.; Choi, H. J.; Kim, K. Structure and Thermal Behavior of a Layered Silver Carboxylate. *J. Phys. Chem. B* **2002**, *106*, 2892−2900.
(38) Lu, Y.; Miller, J. D. Carboxyl Stretching Vibrations of Spontaneously Adsorbed and LB-Transferred Calcium Carboxylates as Determined by FTIR Internal Reflection Spectroscopy. *J. Colloid Interface Sci.* **2002**, *256*, 41−52.
(39) Kim, S.; Chen, L.; Johnson, J. K.; Marand, E. Polysulfone and Functionalized Carbon Nanotube Mixed Matrix Membranes for Gas Separation: Theory and Experiment. *J. Membr. Sci.* **2007**, *294*, 147−158.
(40) Nayak, L.; Rahaman, M.; Khastgir, D.; Chaki, T. K. Thermal and Electrical Properties of Carbon Nanotubes Based Polysulfone Nanocomposites. *Polym. Bull.* **2011**, *67*, 1029−1044.
(41) Milliman, H. W.; Sánchez-Soto, M.; Arostegui, A.; Schiraldi, D. A. Structure−property Evaluation of Trisilanolphenyl POSS/Polysulfone Composites as a Guide to POSS Melt Blending. *J. Appl. Polym. Sci.* **2012**, *125*, 2914−2919.
(42) Volkova, T. S.; Beider, E. Y. Preparation of a Polysulfone-Based Polymer-Silicate Nanocomposite. *Theor. Found. Chem. Eng.* **2011**, *45*, 717−725.
(43) Silberberg, A. Distribution of Segments Near the Surface of a Melt of Linear Flexible Macromolecules: Effect on Surface Tension. *J. Colloid Interface Sci.* **1988**, *125*, 14−22.
(44) Müller, M. Polymers at Interfaces and Surfaces and in Confined Geometries. In *Polymer Science: A Comprehensive Reference*; Matyjaszewski, K.; Möller, M., Eds.; Elsevier: Oxford, U.K., 2012; Vol. *1*.
(45) Brown, H. R.; Russell, T. P. Entanglements at Polymer Surfaces and Interfaces. *Macromoelcules* **1996**, *29*, 798−800.
(46) Arndt, M.; Stannarius, R.; Groothues, H.; Hempel, E.; Kremer, F. Length Scale of Cooperativity in the Dynamic Glass Transition. *Phys. Rev. Lett.* **1997**, *79*, 2077−2080.
(47) Roovers, J.; Ethier, R.; Toporowski, P. M. The Properties of "RADEL R" Polysulfone. *High Perform. Polym.* **1990**, *2*, 151−163.
(48) Wu, S. Chain Structure, Phase Morphology, and Toughness Relationships in Polymers and Blends. *Polym. Eng. Sci.* **1990**, *30*, 753−761.
(49) Kurata, M.; Tsunashima, Y. Viscosity-Molecular Weight Relationships and Unpertutbed Dimensions of Linear Molecules. In *Polymer Handbook*; Brandrup, J., Immergut, E. H., Grulke, E. A., Eds.; John Wiley & Sons, Inc.: New York, 1999; p 52.
(50) Mills, N. J. The Role of Entanglement Networks in the Fracture of Polysulfone. *Rheol. Acta* **1974**, *13*, 185−190.
(51) Eduljee, R. F.; McCullough, R.. Elastic Properties of Composites. In *Materials Science and Technology: A Comprehensive Treatment*; Cahn, R. W.; Haasen, P.; Kramer, E. J., Eds.; Wiley−VCH Verlag GmbH: Weinheim, Germany, 1993; p 381.
(52) Chen, J.; Chen, P.; Wu, L.; Zhang, J.; He, J. Enhanced Fibrillation of LCP by CaCO3 Whisker in Polysulfone Matrix through Increasing Elongational Stress. *Polymer* **2006**, *47*, 5402−5410.
(53) Chen, J.; Chen, P.; Wu, L.; Zhang, J.; He, J. Fibrillation of Liquid Crystalline Polymer in Polysulfone Promoted by Increased System Elasticity via Adding Nano-Silica. *Polymer* **2007**, *48*, 4242−4251.
(54) Fu, S. Y.; Feng, X. Q.; Lauke, B.; Mai, Y. W. Effects of Particle Size, Particle/matrix Interface Adhesion and Particle Loading on Mechanical Properties of Particulate−Polymer Composites. *Composites, Part B* **2008**, *39*, 933−961.
(55) Young, R. J.; Beaumont, P. W. R. Failure of Brittle Polymers by Slow Crack Growth. *J. Mater. Sci.* **1977**, *12*, 684−692.
(56) Ikhlaq, A.; Brown, D. R.; Kasprzyk-Hordern, B. Mechanisms of Catalytic Ozonation on Alumina and Zeolites in Water: Formation of Hydroxyl Radicals. *Appl. Catal., B* **2012**, *123−124*, 94−106.
(57) Edgecombe, S. R.; Gardiner, J. M.; Matsen, M. W. Suppressing Autophobic Dewetting by Using a Bimodal Brush. *Macromolecules* **2002**, *35*, 6475−6477.
(58) Green, D. L.; Mewis, J. Connecting the Wetting and Rheological Behaviors of Poly(dimethylsiloxane)-Grafted Silica Spheres in Poly(dimethylsiloxane) Melts. *Langmuir* **2006**, *22*, 9546−9553.
(59) Yezek, L.; Scha, W.; Chen, Y.; Gohr, K.; Schmidt, M. Influence of Hair Density and Hair Length on Interparticle Interactions of Spherical Polymer Brushes in a Homopolymer Matrix. *Macromolecules* **2003**, *36*, 4226−4235.
(60) Matsen, M. W.; Gardiner, J. M. Autophobic Dewetting of Homopolymer on a Brush and Entropic Attraction Between Opposing Brushes in a Homopolymer Matrix. *J. Chem. Phys.* **2001**, *115*, 2794−2804.